IRAQI Academic Scientific Journals

SAMARRA JOURNAL OF ENGINEERING SCIENCE AND RESEARCH

S.J.E.S.R

Theoretical Nonlinear Analysis of Composite (Pultruded GFRP I-Section and Deck Concrete) Strengthened with GFRP Stiffness

Muataz Ibrahim Ali [1,2*], Abbas A. Allawi [1]

1- Dept. of Civil Engineering, College of Engineering, University of Baghdad, Baghdad, Iraq.
2- Dept. of Civil Engineering, College of Engineering, University of Samarra, Samarra, Iraq.

Article Information
Received: 13/03/2024
Accepted: 31/03/2024
Keywords:
Nonlinear behavior, GFRP, composite beam, Karpenko model, Correia model.

Corresponding Author
E-mail: muitaz88@gmail.com
Mobile: 07837805100

Abstract

This research paper examines the nonlinear behavior of a Glass Fiber-Reinforced Polymer (GFRP) beam when combined with a concrete slab. The investigation is conducted by analyzing the variable modulus of elasticity of the materials, employing Karpenko's model. The paper comprehensively elucidates the outcomes derived from experimental inquiries into the system dynamics of I-section GFRP. The composite structure consists of concrete slabs cast on top of GFRP beams, which are joined using shear connectors in bolts to ensure full interaction. The maximum failure load was determined based on theoretical calculations, and the stiffness calculations for GFRP material were confirmed by testing beams with a net length of 2600 mm with the following variables: type of concrete (normal and high concrete) and the effect of using GFRP T-sections fixed with bolts and epoxy. The results showed that high-strength concrete increased the failure load by 98% compared to its counterpart. The study focuses on finding a mathematical model based on the Karpenko model, which is used to analyze concrete and GFRP composite beams efficiently. Using the results to establish design principles and standards for concrete and GFRP composite structures, the Karpenko model is a remarkable agreement between the numerical, experimental, and theoretical results.

1- Introduction

Fibre-reinforced polymer (FRP) composites have increased in structural applications and structures in the construction industry, especially for structural engineering applications, due to their distinctive properties that attracted engineers. These properties include chemical resistance, corrosion resistance, high hardness and rigidity, and improved static properties. Reduced weight, fatigue strength, and improved damping capabilities **[1, 2]**. Polymer sections have been used in experimental structural parts by examining prismatic sections composed of fiber-reinforced polymer (FRP) materials to achieve composite properties (concrete and FRP sections). As mentioned above, the tendency has been seen in conjunction with the growing utilization of Fibre Reinforced Polymer (FRP) in many applications, encompassing both existing and emerging contexts within concrete constructions.

Studies and scientific research on hybrid beams have been conducted in depth **[1, 3, 4],** which consist of molded polymer composites (FRP) immersed in concrete. These studies have demonstrated and aimed to understand the behavior of composite beams by systematically studying this behavior with theoretical studies (mathematical models) for beams made of (FRP),

which included coated and non-coated beams, where the results showed an improvement in the bearing capacity of the coated beams compared to the behavior of the non-coated beams **[5]**.

In addition, beams coated with concrete improved ductility more than beams that were not coated **[6-8],** as some previous research showed that the bond between concrete and (FRP) components with lengths of 750 mm and 500 mm showed that bending decreased with an increase in failure loads, compared to uncoated beams **[9]**.

Shear connectors between the GFRP beam and the concrete slab have a significant impact on the results of the tests (amount of deflection and failure strength) through studies presented by researchers and different types and methods of shear connectors for (GFRP) beams with concrete, such as the study presented **[10]**, which evaluated the use of sand-coated fiberglass reinforced polymer (GFRP) nails instead of steel nails, which contributed to significantly reducing slip and thus improving the bending properties of the composite beams. Kavlicoglu B. et al. **[11]** investigated the flexural properties of beams fabricated using a composite material consisting of (GFRP) and concrete, employing both analytical and experimental techniques.

Many constitutive relationships have been suggested to represent the stress-strain characteristics of concrete and steel. Nevertheless, several correlations have failed to consider crucial mathematical and physical factors. For example, certain connections exclusively depict the upward portion of concrete subjected to compression, while others do not adequately portray the stress-strain diagram for concrete experiencing tension **[12]**.

In 1986, Korpenko **[13]** colleagues introduced a mathematical model to establish a connection for forecasting the stress-strain behavior of concrete and steel under uniaxial loads. The above-described association garnered substantial attention due to its ability to efficiently tackle most of the abovementioned difficulties. Moreover, this correlation has facilitated the standardization of the stress-strain diagram depiction for both tensile and compressive behavior of concrete and various steel grades, such as mild and high-strength steel.

Since the discovery of concrete strength augmentation **[14],** concrete behavior has been studied extensively. Some models were based on biaxial compression studies **[15]**, while others were based on a limited quantity of constrained concrete softening data **[16]**. Concrete compressive behavior has been thoroughly explored through recent triaxial compression studies **[17]**, creating a complete database. This database can build and validate constrained concrete models. An extensive collection of experimental research has been used to develop models for steel-confined concrete's axial stress-strain behavior **[18]**. The level of confinement, dictated by the lateral reinforcement ratio and uniaxial compressive strength, affects the ultimate strength and stress-strain curve descending area. Given the advances in high-strength concrete, steel, and composite materials (FRPs) as confining reinforcement, these models' limitations require improved calibrations. This drove the creation of alternate conventional and high-strength concrete models **[19].** If localization is not considered, the softening zone will impact size regardless of the function, making objective results unattainable **[20]**. The compressive softening zone is usually regularised in finite element calculations using constant fracture energy criteria, comparable to tensile cracking in concrete **[21]**.

Plasticity-based models use constitutive drivers or finite element analysis to describe concrete hardening, softening, and dilatation **[22]**. Finite element analysis methods using concrete plasticity models are ideal for constructions with complex geometry and boundary conditions. Structural engineers may prefer simpler models in the preliminary design of loaded concrete elements with varied constitutive relationships to estimate (load– deformation) behavior **[23]**.

The behavior of the beams is predicted using an analytical model that includes force equilibrium, strain compatibility, FRP linear elastic properties, and a concrete partial stress-strain confinement model **[24]**. An analysis model was presented based on applied stresses, strain compatibility, and linear elastic properties of FRP, as well as stress and strain of concrete, to predict the behavior of composite beams **[25]**; the model demonstrated a convergence of

compatibility between practical models and the predictive model for use in increasing the adaptability of GFRP sections **[26].**

The most prominent failure case for GFRP beams is the failure that occurs at the point of intersection of the edge web and inside the web when used in composite beams. The theoretical study of the causes of shear failure and the factors influencing this failure is the goal of the current study, which aims to address the causes of failure (shear failure at the point of intersection between the edge and the web and crushing) and see how well the proposed mathematical model matches the practical results.

2- Materials and Sample Preparation

The experimental setting tested the structure of GFRP I-sections with a concrete slab. The results were compared to theoretical predictions. The GFRP I-section is 100 × 150 mm and has a 10 mm flange and web thickness. The experiment used two 2600-mm beams. The beams were manufactured from GFRP T-sections connected with epoxy and bolts. The beams were made of 0.5-mm corrugated metal sheets to simulate real-life conditions. The slab specimens can be divided into 20.1 MPa normal compressive strength concrete (NCC) and 52.3 MPa high compressive strength concrete HCC. The concrete models were water-cured for 28 days. The beams were split and joined to the rigidity T-section GFRP using bolts and epoxy after 14 days of cure. The composite structure was then cured in ambient air for 14 days.

Before the bonding procedure, the surfaces of the stiffness T-section GFRP and I-section GFRP beams were subjected to surface preparation by sandpaper abrasion. After mixing, the adhesives were applied to both surfaces and later connected. After completing the bonding process, the specimens were exposed to the ambient atmosphere for a curing period of 14 days before undergoing testing.

Two mechanical shear connectors are utilized as bolts in a complete shear connection without slippage. These bolts have dimensions of 40 mm in length and 8 mm in diameter and possess a yield strength (fy) of 630 MPa. They serve the purpose of connecting a GFRP beam to a slab, as well as securing corrugated metal sheets. A 75 mm long and 12 mm diameter component, possessing a yield stress of 630 MPa, is employed to affix the GFRP stiffener to the GFRP beam. Before pouring the concrete slab, all the (GFRP) specimens were attached using bolts in Figure 1. Show the details of the loading on the composite beam and details of the stiffeners. Table (1) shows details of the nomenclature of the models in terms of bonding method and type of slab concrete.

Table (1): Details of the nomenclature of the models

Specimen No.	Type Concrete	Bond Epoxy	Bond Bolts
HNEB	Normal	ok	ok
HHEB	High	ok	ok

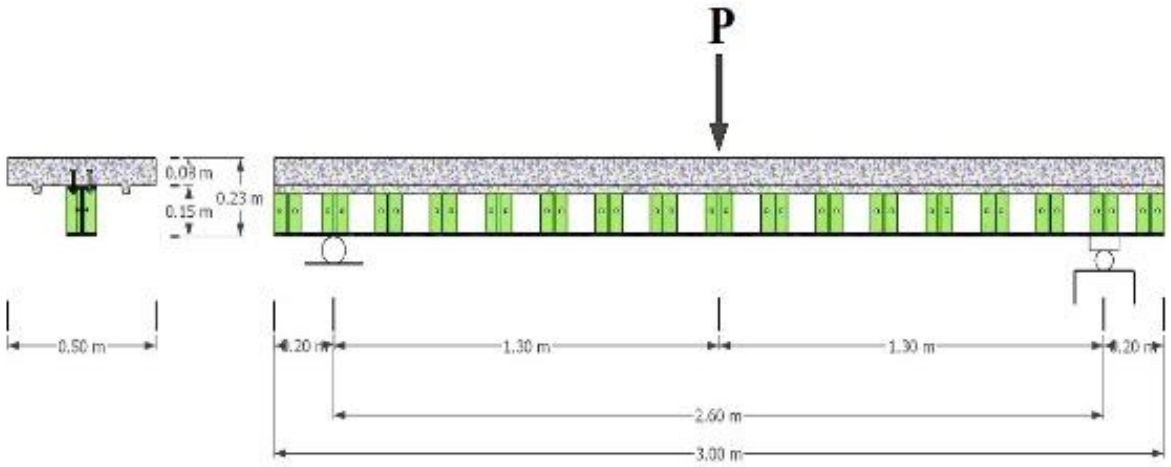

Figure 1. Details of the loading on the composite beam.

3- Testing Procedures

In the case of a fully bonded shear connection without any slippage, two mechanical shear connectors are employed in the shape of bolts. The bolts under consideration exhibit dimensions of 40 mm in length and 8 mm in diameter, together with a yield strength (fy) of 630 MPa. These components facilitate the connection between a (GFRP) beam and a slab while also providing the means to fasten corrugated metal sheets. The element for attaching the GFRP stiffener to the GFRP beam is a cylindrical object with a length of 75 mm and a diameter of 12 mm. It has a yield stress of 630 MPa. All the (GFRP) specimens were attached using bolts before pouring the concrete slab.

4- Design of GFRP Stiffeners

Stiffeners are supplementary plates or sections attached to the webs or flanges of beams to augment their resistance to deformations outside the beam's plane. The critical component that influences the flexural stress of the GFRP section is the occurrence of local buckling in its conspicuous flange **[27]**. In order to mitigate the occurrence of buckling during the testing process, the integration of (GFRP) stiffeners is implemented, as per the South African National Standards (SANS) **[28]**. Figure 2 illustrates the representation of the stiffener and the associated methodology for its immobilization in a stationary state. The stiffeners are constructed as a vertical element within the I-Section beam, consisting of two distinct components: the bearing strength (Br) and the compressive resistance (Cr). The necessity for bearing stiffeners arises at both ends of a structure, particularly when the tension field lacks sufficient anchorage **[28-30]**. The design of the columns will incorporate a pair of stiffeners and a centrally positioned web strip per the specifications provided in SANS 10162-1 **[28-30]:**

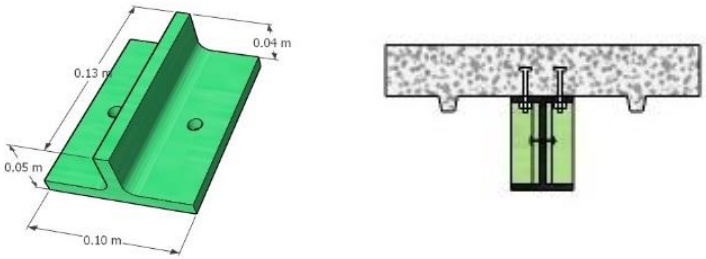

Figure 2. Details of the stiffeners.

After determining the minimum value of (Cu) from (Br, Cr) by comparing it with the values acquired from the experimental analysis of the (GFRP) model, as depicted in Figure (2), the T-shape is utilized. The flange, measuring 100*10 mm, and the web, measuring 35*10 mm, are reinforced with stiffeners. The stiffeners are spaced at intervals of 185 mm beneath the loading point.

Figure (2): compressive test of (GFRP) model **[28]**.

5- Full Shear Connection

Applying external forces to the composite beam results in discernible structural failures. The failure modes seen in this study encompass bottom flange flexural failure caused by tension, fracture, or shear stresses, local web buckling resulting from compressive forces, and shear failure. The structural system encompasses various modes: local web buckling induced by compressive stresses, concrete shear failure, concrete compressive failure, global concrete failure due to lateral buckling, and interface shear connection failure. In this study, all instances of failure were attributed to web shear. The beam size was selected to induce compression in the concrete and achieve alignment of the neutral axis with the slab. The hybrid beam was studied by researcher Correia **[31]**, who used the composite section equations to analyze. According to the hypothesis, the concrete in the beam reaches the point of failure, which is a compressive failure in the concrete.

6- Nonlinear Analysis

The approach proposed for analyzing composite beams in the nonlinear state includes the following under different loading conditions (including service loads until failure is reached) by relying on the nonlinear analysis of the Karpenko model, which depends on a variable coefficient of elasticity modulus values with each load case. The stresses along the section can be determined at each loading stage using the Karpenko relationships **[13]**, which describe the strain-stress behavior of both concrete and steel bars. The modulus of elasticity of a (GFRP) material remains relatively constant during the loading phase until it reaches the point of failure due to the nearly linear relationship between strain and stress **[32]**.

7- Stress-strain theoretical model

Korpenko proposed a theoretical framework to establish the correlation between stress and strain in concrete and steel subjected to uniaxial stresses. The relationship mentioned above gained significant popularity due to its ability to effectively address most of the abovementioned challenges. As depicted in Figure 3, the stress-strain diagram of concrete is characterized by Equations (1) to (6), which incorporate the equations for the coefficients. v_m and e_{1c}.

$$\hat{v}_c = \frac{f_c'}{|\varepsilon_u| E_c} \quad ; \varepsilon_{c,el} = 0 \tag{1}$$

$$v_o = 1 \quad ; \varepsilon_u \leq 1$$
$$v_o = 2.05\hat{v}_c \quad ; \varepsilon_u > 1 \tag{2}$$

$$e_{1c} = 1.72 - 1.82\hat{v}_c \quad ; \varepsilon_u \le 1$$
$$e_{1c} = 1.95\hat{v}_c - 0.138 \quad ; \varepsilon_u > 1 \tag{3}$$

$$\eta_c = \frac{f_c - f_{c,el}}{f'_c - f_{c,el}} \quad ; \; f_{c,el} = 0 \tag{4}$$

$$e_{2c} = 1 - e_{1c} \tag{5}$$

$$v_c = 1 \quad ; |f_c| \le |f_{c,el}|$$

$$v_c = \hat{v}_c \pm (v_o - \hat{v}_c)\sqrt{1 - e_{1c}.\eta_c - e_{2c}.\eta_c^2}, \tag{6}$$

$$when: \quad |f_c| > |f_{c,el}|$$

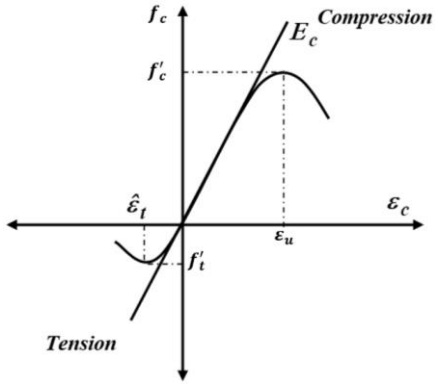

Figure 3: Stress-strain diagram for concrete **[32].**

8- The Neutral Axis Depth

In most cases, including the case of the analysis of the composite section by the researcher **(Correia et al., 2013)**, the analysis is adopted before the occurrence of cracking (linear case) and the analysis when the concrete reaches the state of failure (crushing). Through Equation. (7) and Equation. (8), Figure (4) shows details of the step calculation of the neutral axis depth.

$\boldsymbol{X_u}$= The ultimate neutral axis depth in case of failure, the calculation of the final neutral axis depth, assuming a full shear connection between bolts (shear connectors), is determined by evaluating the neutral axis depth (Xu) using Equation (10). This phenomenon is depicted in Figure 5.

$$k_1 = \frac{\sum f_{ci}.\varepsilon_i}{\sum \varepsilon_i . f_{c\,n}} \tag{7}$$

$$k_2 = 1 - \frac{\sum f_{ci}.\varepsilon_i}{\varepsilon_u.\sum f_{ci}} \tag{8}$$

$$[(k_1.[(1-k_2).\varepsilon_c.v_c.E_c)].b_c.X].X + [A_p.E_p.\varepsilon_c].X - A_p.E_p.\varepsilon_c.\left(\frac{h}{2} + h_c\right) = 0 \tag{9}$$

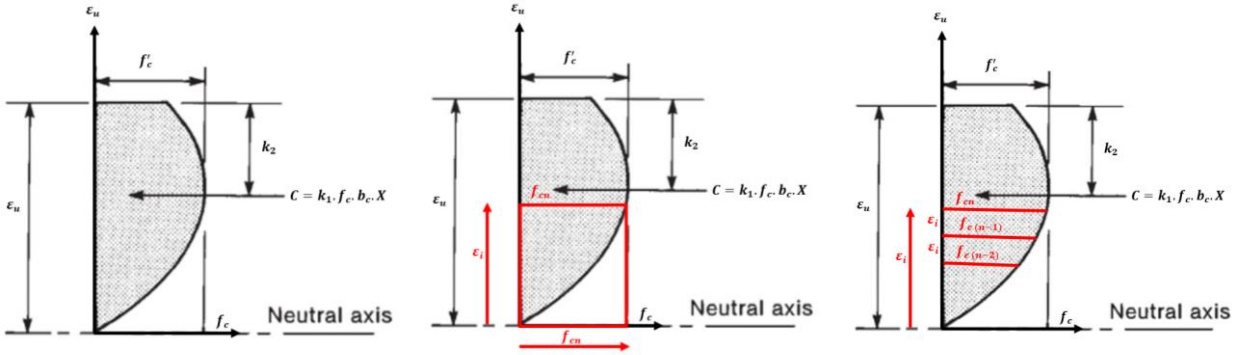

Figure (4): Details of calculating the neutral axis depth at any load.

$$(\boldsymbol{0.8\,.fc'.b_c.X_u}).\boldsymbol{X_u} + \left(\boldsymbol{A_p.E_p.\varepsilon_c}\right).\boldsymbol{X_u} - \boldsymbol{A_p.E_p.\varepsilon_c}.\left(\frac{\boldsymbol{h}}{\boldsymbol{2}} + \boldsymbol{h_c}\right) = \boldsymbol{0} \tag{10}$$

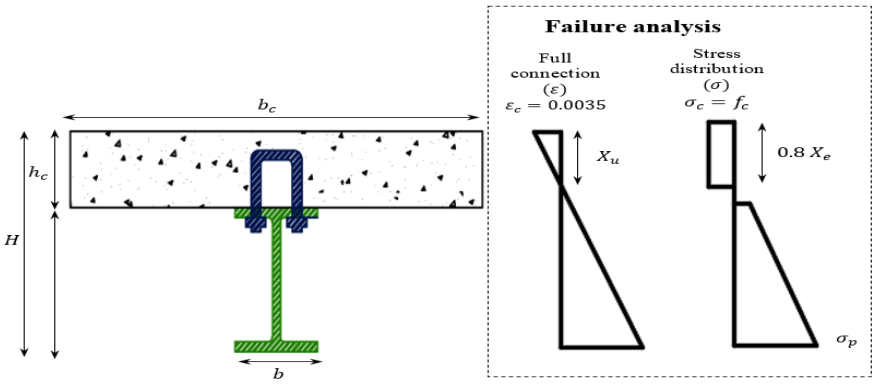

Figure (5): Details calculation of the ultimate neutral axis depth **[31].**

9- Calculating Load:

The flexural Load is calculated from the bending moment; in the case of this study, the composite beam is simply supported (s.s) as in Equation (8). For ultimate Load, use Correia's Equation by using the equivalent rectangular block with a value (0.8) of compressive strength and the value of strain, taking into account $\boldsymbol{\varepsilon_c = \varepsilon_{cu}} = 0.0035$, using Equations (11) and Equation (12).

$$p_i = \frac{4 * M_i}{\mathrm{L}} \tag{11}$$

$$M_u = (0.8 * b_c * X_u * f_c) * (0.6 * X_u) + \left(A_f * E_p\right) * \left[\frac{\varepsilon_c}{X_u} * (h_c + \frac{t_f}{2} - X_u)\right] * (h_c + \frac{t_f}{2} - X_u) + \left(A_w * E_p\right) * \left[\frac{\varepsilon_c}{X_u} * (\frac{h}{2} + h_c - X_u)\right] * (\frac{h}{2} + h_c - X_u) + \left(A_f * E_p\right) * \left[\frac{\varepsilon_c}{X_u} * (h + h_c - \frac{t_f}{2} - X_u)\right] * (h + h_c - \frac{t_f}{2} - X_u) \tag{12}$$

In the case of Load between non-load and ultimate Load (nonlinear), Equation (7) and Equation (8) to find the neutral axis depth of compressive concrete at any load (X) to find the bending moment is used Equation (13). So, the theoretical analysis result of all beams is shown in Table (2). The failure load depended on the shear failure in the web of the GFRP beam when using the same strain shear failure value on the web for the experimental test.

$$M_u = \left[\left((1 - k_2).\varepsilon_c.v_c.E_c.k_1\right).b_c.X\right] * [(1 - k_2).\mathrm{X}] + \left(A_f * E_p\right) * \left[\frac{\varepsilon_c}{X} * (h_c + \frac{t_f}{2} - \mathrm{X})\right] * (h_c + \frac{t_f}{2} - \mathrm{X}) + \left(A_w * E_p\right) * \left[\frac{\varepsilon_c}{\mathrm{X}} * (\frac{h}{2} + h_c - \mathrm{X})\right] * (\frac{h}{2} + h_c - \mathrm{X}) + \left(A_f * E_p\right) * \left[\frac{\varepsilon_c}{\mathrm{X}} * (h + h_c - X_u - \frac{t_f}{2})\right] * (h + h_c - X_u - \frac{t_f}{2}) \tag{13}$$

10- Maximum Deflection:

The total deformation of hybrid beams, which consist of Glass Fibre fiber-reinforced polymer (GFRP) and concrete, is influenced by two primary elements. Firstly, the deflection resulting from bending is considered, considering the deflection's flexibility. Secondly, the connection induced by shear is taken into consideration. In order to ascertain the maximum deflection, it is necessary to initially calculate the value ($n = {E_c}/{E_p}$), where the modulus of elasticity (E_c) gets it by Equation. (14), it is necessary to ascertain the depth of the neutral axis ($X_{,el}$) found according to Equation. (15), use Equation before the strain in the bottom edge concrete slab reaches a near value (0.0004). Equation. (16) to find the section's equivalent inertia (I_{eq}^{GFRP}), and after that, use Equation. (9), as well as the section's equivalent inertia (I_{eq}^{GFRP}) by using Equation (17).

The distribution of a shear load on the beam occurs at the interface between the concrete slab and the GFRP beam. It is important to acknowledge that the shear deformation in this situation is

significant. A hypothesis with a conservative perspective is proposed, suggesting that the web of a profile solely carries the shear force. Based on the assumption mentioned above, determining the maximum deflection of GFRP-concrete hybrid beams with simple support, under the influence of a point load (P) applied at any position along its span, can be achieved by utilizing Equation (14), used to find deflection at any load use Equation (18).

The value of shear rigidity equals approximately 10 % of the modulus of elasticity. (E_p) for the GFRP beam **[27]**. The theoretical analysis findings regarding defecation for all beams are presented in Table 2.

$$E_c = .E_c' \quad ; E_c' = 4700\sqrt{f_c'} \tag{14}$$

$$X_{,el} = \frac{A_p * \left(h_c + \frac{h}{2}\right) + n * A_c * \frac{h_c}{2}}{A_p + n * A_c} \tag{15}$$

$$I_{eq}^{GFRP} = \frac{n * A_c * h_c^2}{12} + n * A_c * \left(X_{,el} - \frac{h_c}{2}\right)^2 + I_p + +A_p * (h_c + \frac{h}{2} - X_{,el}) \tag{16}$$

$$I_{\text{eq}}^{\text{GFRP}} = \frac{n \times b_{\text{c}} \times X_{,\text{el}}^3}{3} + I_{\text{p}} + A_{\text{p}} \times \left(h_{\text{c}} + \frac{h}{2} - X_{,\text{el}}\right)^2 \tag{17}$$

$$\delta = \frac{P * L^3}{48 * EI_{eq}^{GFRP}} \left(\frac{\delta_P}{\delta_f}\right) + \frac{P * L}{4 * G_p * A_w} \tag{18}$$

Table 2. Results of theoretical analysis.

Specimen No.	Ultimate strain	Failure load (kN)	Mid deflection (mm)	Strain Failure test	Failure load (kN)	Mid deflection (mm)
HNEB	0.0035	121.63	48.39	0.0010	70.33	27.98
HHEB	0.0035	218.55	83.67	0.0012	125.18	48.30

11- Results and Discussion

a. Maximum Load Failure

Table (3) displays the flexural outcomes of all the analyzed beams. The experimental results indicated that the failure load of the composite beams, which were reinforced with GFRP T-Section stiffness and fixed using a combination of bolts and epoxy, along with slab casting using standard concrete with a compressive strength of 20.1 MPa, exhibited a more significant failure load compared to the beams reinforced with slab casting using high concrete with a compressive strength of 52.3 MPa, with an increase of 98 %.

Table 3. Results of experimental test.

Specimen No.	Failure load (kN)	Mid deflection (mm)	Strain Failure	Mode Failure
HNEB	66.820	28.10	0.001	Shear web
HHEB	120.20	50.22	0.0012	Shear web

The theoretical analysis yielded results that closely aligned with the experimental findings of the HNEB and HHEB beams. However, the experimental results were unexpectedly lower due to shear web failure (Splitting the web into two parts in the middle) during the installation of the GFRP T-Section stiffness, specifically when creating holes for the bolts in the web. Figure 6 illustrates the disparity in outcomes between theoretical calculations and experimental test values.

b.Maximum Deflection

Tables 2 and 3 present the maximum deflection values obtained from the experimental analysis of the beams under investigation, with the corresponding theoretical predictions. The discrepancy in deflection ratios between the HNEB and HHEB beams can be attributed to variations in the compressive strength of the concrete. A lower compressive strength results in a reduced modulus of elasticity, leading to a shallower compression zone depth. It is important to note that failure in all beams did not occur due to concrete crushing or tensile failure of the GFRP beam. The failure occurred explicitly in the web of the composite beams, resulting in shear failure. This can be attributed to the inherent weakness of the web area. Figure 7 illustrates the load-deflection curve of the composite beams, indicating that the beams with normal strength casting exhibit lower deflection compared to those with high concrete slab casting. The model based on the Korpenko model demonstrates a satisfactory level of agreement between the numerical model (Korpenko) and experimental results. However, the researcher Correia analyses **[33]** the hybrid beam model using composite section equations, assuming that the concrete reaches the failure stage (compression failure). The latter model indicates a linear relationship between the load-deflection curve, which lacks logical consistency as materials typically do not exhibit linearity throughout all load steps.

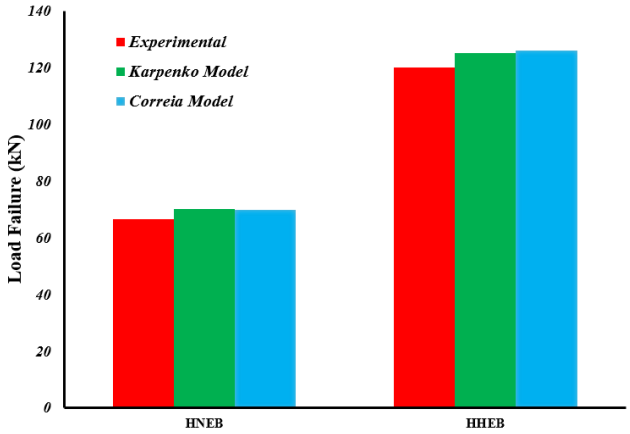

Figure 6. Theoretical calculations vs. experimental test.

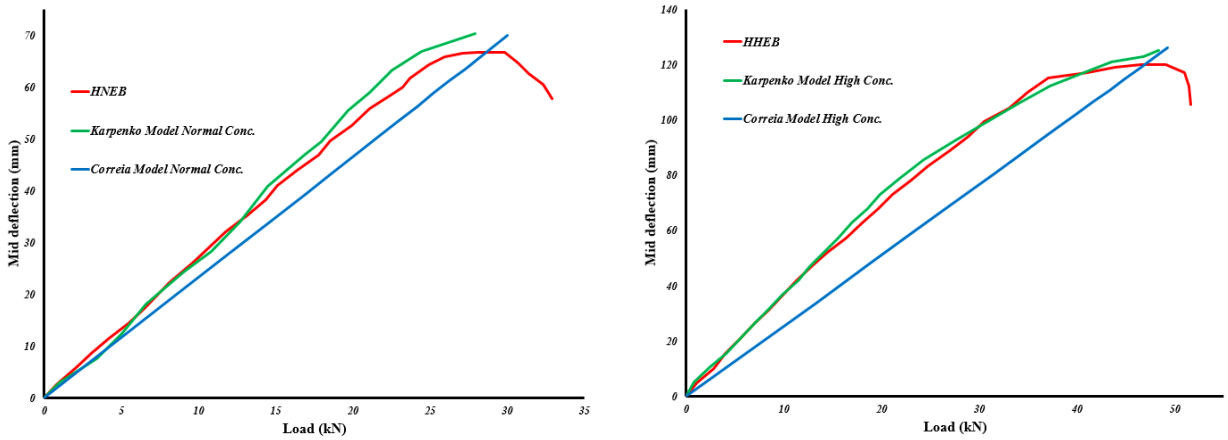

a. Normal strength concrete b. High-strength concrete

Figure 7. Mid deflection vs. applied Load for composite beams.

c. Strains

Figure 8 illustrates the strains observed in the two beams under investigation, specifically the strain levels at the top concrete slab while loading the HNEB and HHEB beams. A comparison is made between composite beams with slab casting using higher compressive strength (HCC) and those with normal compressive strength (NCC). The analysis reveals that the higher compressive strength increases strain, which can be attributed to the higher flexural Load required to reach

the failure load. The ratio experienced a 20% increase when comparing the high-strength concrete (HCC) with the normal concrete (NCC). The strength stiffeners, consisting of epoxy and bolts combined in the composite portion, operate cohesively.

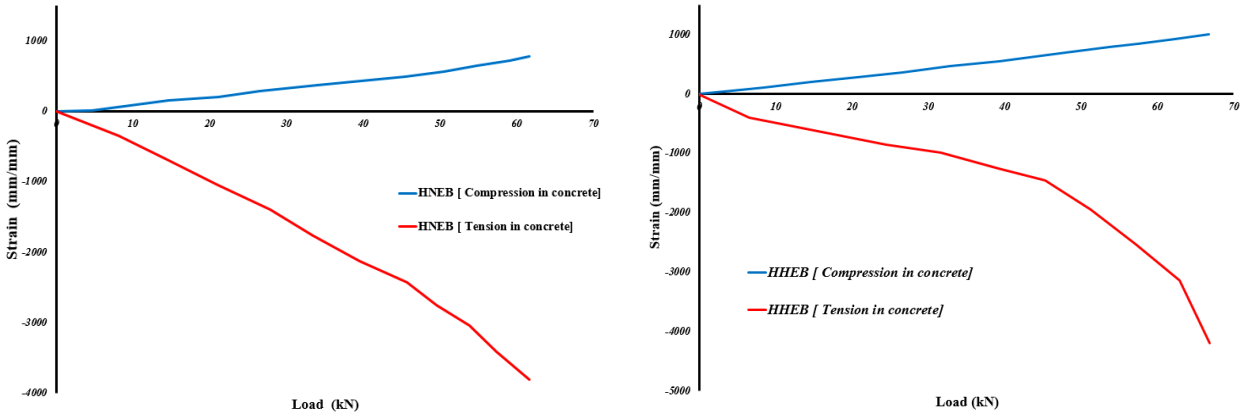

a. Normal strength concrete b. High-strength concrete

Figure 9. Top and Bottom Extreme Fibre Strain (*10^{-6}) vs a load of Composite Beams.

12- Conclusions

Experiments examined the structural behavior of GFRP I-sections with fully bonded concrete slabs. The Korpenko model predictions are compared against experimental data. The shear web of these parts was reinforced with GFRP T-section stiffeners, increasing strength. Epoxy adhesive and mechanical connectors, particularly bolts, achieved enough composite action and delayed shear failure inside the GFRP beam web. The composite beams reinforced with bolts and epoxy had higher ultimate failure stresses than the GFRP beams reinforced with bolts alone. Composite beams have higher tensile strain than GFRP sections assessed using the Korpenko model in the practical test. Proves that GFRP and full hybrid action optimize FRP use in tension and compression in concrete structures. Web shear and fracture in (GFRP) material are the leading causes of composite beam failure. A firm concrete and FRP composite foundation needs more study and analysis to comprehend FRP and concrete; more research is required. The Korpenko model for composite beam analysis also shows a good match between computational and experimental results.

Nomenclature			
A_c	area of the concrete layer	b_f	GFRP flange width.
A_f	area of the GFRP profile flange	b_c	concrete layer width.
A_p	area of the GFRP profile	b_{eff}	effective width of the concrete slab.
A_w	area of the GFRP profile web	b_L	longitudinal spacing of point load.
E_c	Young modulus of the concrete	b_0	shear connectors-spacing.
E_p	Young modulus the longitudinal GFRP	f_c	compressive strength of concrete.
F_c	compressive strength of the concrete slab	f_{su}	ultimate stress of steel.
$F_{s,max}$	maximum shear connection force (from the shear connection test).	n	factor of homogenization.
G_p	GFRP shear-modulus.	t_f	GFRP flange thickness.
H	Height of the hybrid section.	t_w	GFRP web thickness.
I_c	The inertia of the concrete layer is on the principal axis.	h	Height of the GFRP section.
I_{eq}^{GFRP}	equivalent inertia in the GFRP	h_c	Thickness of the concrete layer.
I_p	The inertia of GFRP in the principal axis.	r	distance (centroids of concrete to section components).
K	shear-connection stiffness.	δ_f	Mid-span deflection for full interaction in shear
L	beam span.	δ_p	Mid-span deflection in case of partial shear interaction

M_u	**ultimate moment.**	$\epsilon_{cu}=\epsilon_c$	**Strain at the ultimate of the curve (stress-strain) concrete =0.0035.**
P	**point load.**	b_e	**The effective stiffener width.**
X_{el}	**neutral axis (elastic analysis).**	**s**	**spacing between stiffeners.**
X_u	**neutral axis (at failure).**	f_c	**Target value of compressive strength**
f_{yG}	**specified yield point of the GFRP**	ε_i	**Strain at the center of every area slips from the top edge of the concrete.**
$\emptyset_{bi}$	**0.8**	$\hat{v}_c$	**coefficient of elastic strain when $f_c = f'_c$**
t_v	**the thickness of the stiffener**	E_c	**Initial modulus of elasticity for the concrete.**
v_o	**The coefficient depends on the stress level of the concrete.**	e_{1c}	**A coefficient that depends on the type of materials must $e_{1c} < 2$.**
e_{2c}	**Coefficient that depends on the type of materials $e_{2m} = 1 - e_{1m}$**	k_1	**Coefficient of concrete compressive strength at any load.**
k_2	**Coefficient of the neutral axis depth of the concrete compressive strength at any load.**	f_{ci}	**average of (f_c) from the curve for stress-strain at every slip.**
$f_{c\,n}$	**the target value of the concrete compressive strength (f_c)**	v_m	**Coefficient of elastic strain (represents the elastic strain to the total strain)**

REFERENCES

1. Liu, T., et al., *Flexural behavior of novel hybrid multicell GFRP-concrete beam.* Composite Structures, 2020. **250**: p. 112606.
2. Mahmood, E.M., A.A. Allawi, and A. El-Zohairy, *Flexural Performance of Encased Pultruded GFRP I-Beam with High Strength Concrete under Static Loading.* Materials, 2022. **15**(13): p. 4519.
3. Evbuomwan, N. *Behaviour of FRP prismatic sections in composite action with concrete*. in *International conference on fibre reinforced composites No7, Newcastle upon Tyne*. 1998.
4. Liu, T., X. Liu, and P. Feng, *A comprehensive review on mechanical properties of pultruded FRP composites subjected to long-term environmental effects.* Composites Part B: Engineering, 2020. **191**: p. 107958.
5. Ibrahim, T.H., et al., *Theoretical Analysis of Composite RC Beams with Pultruded GFRP Beams subjected to Impact Loading.* Engineering, Technology & Applied Science Research, 2023. **13**(6): p. 12097-12107.
6. Barbero, E., et al., *Determination of material parameters for Abaqus progressive damage analysis of E-glass epoxy laminates.* Composites Part B: Engineering, 2013. **46**: p. 211-220.
7. Canning, L., L. Hollaway, and A. Thorne, *An investigation of the composite action of an FRP/concrete prismatic beam.* Construction and Building Materials, 1999. **13**(8): p. 417-426.
8. Deskovic, N., U. Meier, and T.C. Triantafillou, *Innovative design of FRP combined with concrete: long-term behavior.* Journal of Structural Engineering, 1995. **121**(7): p. 1079-1089.
9. Zou, X., et al., *A review on FRP-concrete hybrid sections for bridge applications.* Composite Structures, 2021. **262**: p. 113336.
10. Zou, X., et al., *Experimental and analytical studies on shear behaviors of FRP-concrete composite sections.* Engineering Structures, 2020. **215**: p. 110649.
11. Kavlicoglu, B., et al. *Analysis and testing of graphite/epoxy concrete bridge girders under static loading*. in *Proceedings of Conference on Retro-fit and Repair of Bridges, London, England*. 2001.
12. Oukaili, N.K. and A.A. Al-Asadi, *Analysis of Concrete Flexural Members Reinforced with Fibre Polymer.* Journal of Engineering, 2010. **16**(3).
13. Korpenko, N., T. Mukhamediev, and A. Petrov, *The Initial and Transformed Stress-Strain Diagrams of Steel and Concrete.* Special Publication, Stress-Strain Condition for Reinforced Concrete Construction, Reinforced Concrete Research Center, Moscow, 1986: p. 7-25.
14. Richart, F.E., *Study of the failure of concrete under combined compressive stresses.* University of Illinois Engineering Experimental Station, Bulletin, 1928. **185**: p. 104.
15. Madas, P. and A. Elnashai, *A new passive confinement model for the analysis of concrete structures subjected to cyclic and transient dynamic loading.* Earthquake engineering & structural dynamics, 1992. **21**(5): p. 409-431.
16. Ahmad, S. and S.P. Shah. *Stress-strain curves of concrete confined by spiral reinforcement*. in *Journal Proceedings*. 1982.
17. Attard, M. and S. Setunge, *Stress-strain relationship of confined and unconfined concrete.* Materials Journal, 1996. **93**(5): p. 432-442.
18. Assa, B., M. Nishiyama, and F. Watanabe, *New approach for modeling confined concrete. I: Circular columns.* Journal of Structural Engineering, 2001. **127**(7): p. 743-750.

19. Scott, B.D., R. Park, and M.J. Priestley. *Stress-strain behavior of concrete confined by overlapping hoops at low and high strain rates*. in *Journal Proceedings*. 1982.
20. Bazant, Z.P., L. Cedolin, and J. Hutchinson, *Stability of structures: elastic, inelastic, fracture, and damage theories.* 1993.
21. Feenstra, P.H. and R. De Borst, *A composite plasticity model for concrete.* International journal of solids and structures, 1996. **33**(5): p. 707-730.
22. Al-Hawwassi, I.F.P. and N.K.A. Oukaili, *Short term deflection of ordinary, partially prestressed and GFRP bars reinforced concrete beams.* Journal of Engineering, 2010. **16**(1).
23. Pivonka, P., R. Lackner, and H. Mang. *Numerical analyses of concrete subjected to triaxial compressive loading*. in *European Congress on Comp. Methods in Applied Mech*. 2000.
24. Ibrahim, T.H., A.A. Allawi, and A. El-Zohairy, *Impact Behavior of Composite Reinforced Concrete Beams with Pultruded I-GFRP Beam.* Materials, 2022. **15**(2): p. 441.
25. Zhang, P., et al. *Shear performance of the epoxy-bolt interface between UHPC slabs and GFRP girder*. in *Structures*. 2023. Elsevier.
26. Ibrahim, T.H., A.A. Allawi, and A. El-Zohairy, *Experimental and FE analysis of composite RC beams with encased pultruded GFRP I-beam under static loads.* Advances in Structural Engineering, 2023. **26**(3): p. 516-532.
27. Allawi, A.A. and S.I. Ali, *Flexural behavior of composite GFRP pultruded I-section beams under static and impact loading.* Civ. Eng. J, 2020. **6**: p. 143-2158.
28. Nkosi, G.M., *A reliability based comparison of Eurocode 3 & SANS 10162-1*. 2020: University of Johannesburg (South Africa).
29. Ali, S.I. and A.A. Allawi, *Effect of Web Stiffeners on the Flexural Behavior of Composite GFRP Concrete Beam Under Impact Load.* Journal of Engineering, 2021. **27**(3): p. 73-92.
30. Mahachi, J., *Calibration of partial resistance factors for cold-formed steel in South Africa.* 2018.
31. Correia, J.R., et al., *Mechanical behaviour of pultruded glass fibre reinforced polymer composites at elevated temperature: Experiments and model assessment.* Composite Structures, 2013. **98**: p. 303-313.
32. Oukaili, N., *Moment capacity and strength of reinforced concrete members using stress-strain diagrams of concrete and steel.* Journal of King Saud University, 1997. **10**: p. 23-44.
33. Correia, J.R., F.A. Branco, and J.G. Ferreira, *Flexural behaviour of GFRP–concrete hybrid beams with interconnection slip.* Composite Structures, 2007. **77**(1): p. 66-78.